Monthly Notices
of the
ROYAL ASTRONOMICAL SOCIETY

MNRAS **460,** 356–362 (2016)
Advance Access publication 2016 April 21

doi:10.1093/mnras/stw922

Oscillator strengths for high-excitation Ti II from laboratory measurements and calculations

H. Lundberg,[1] H. Hartman,[2,3]★ L. Engström,[1]★ H. Nilsson,[3]★ A. Persson,[1] P. Palmeri,[4] P. Quinet,[4,5] V. Fivet,[4] G. Malcheva[6] and K. Blagoev[6]

[1]*Department of Physics, Lund University, PO Box 118, SE-221 00 Lund, Sweden*
[2]*Applied Mathematics and Material Science, Malmö University, SE-20506 Malmö, Sweden*
[3]*Department of Astronomy and Theoretical Physics, Lund University, PO Box 43, SE-221 00 Lund, Sweden*
[4]*Physique Atomique et Astrophysique, Université de Mons, B-7000 Mons, Belgium*
[5]*IPNAS, Université de Liège, B-4000 Liège, Belgium*
[6]*Institute of Solid State Physics, Bulgarian Academy of Sciences, 72 Tzarigradsko Chaussee, BG-1784 Sofia, Bulgaria*

Accepted 2016 April 18. Received 2016 April 18; in original form 2016 January 27

ABSTRACT

This work reports new experimental radiative lifetimes of six $3d^2(^3F)5s$ levels in singly ionized titanium, with an energy around 63 000 cm^{-1} and four $3d^2(^3F)4p$ odd parity levels where we confirm previous investigations. Combining the new 5s lifetimes with branching fractions measured previously by Pickering et al., we report 57 experimental log *gf* values for transitions from the 5s levels. The lifetime measurements are performed using time-resolved laser-induced fluorescence on ions produced by laser ablation. One- and two-step photon excitation is employed to reach the 4p and 5s levels, respectively. Theoretical calculations of the radiative lifetimes of the measured levels as well as of oscillator strengths for 3336 transitions from these levels are reported. The calculations are carried out by a pseudo-relativistic Hartree–Fock method taking into account core-polarization effects. The theoretical results are in a good agreement with the experiments and are needed for accurate abundance determinations in astronomical objects.

Key words: atomic data – methods: laboratory: atomic.

1 INTRODUCTION

Lines from the iron-group elements are among the most abundant in spectra of astronomical objects. In the B, A and F class stars, the first ions of Fe, Cr and Ti dominate the ultraviolet and visible spectrum. Even so-called forbidden lines in Ti II have been found to be very intense in the strontium filament ejecta of the massive star Eta Carinae (Hartman et al. 2004). Titanium is located among the lighter of the iron-group elements and is considered primarily to be an α-element, i.e. produced by successive captures of He nuclei through among others, Mg, Si and Ca. Recent studies of metal-poor stars, however, show trends where the titanium abundance is correlated with scandium and vanadium indicating a similar production mechanism as the iron-group elements rather than the α-elements (Sneden et al. 2016). Accurate atomic data are needed to reliably determine the Ti abundance in these objects.

The ground term in Ti II is $3d^24s\ ^4F$, followed by even terms belonging to the $3d^24s$, $3d^3$ and $3d4s^2$ configurations up to an energy of 25 000 cm^{-1}. The lowest odd configurations are $3d^24p$ and $3d4s4p$ spanning the energy interval from 29 500 to 59 500 cm^{-1} (Huldt et al. 1982). Transitions between these configurations give rise to the most intense spectral lines in Ti II, and have been the subject of most previous experimental and theoretical investigations. The higher lying even configurations $3d^25s$, $3d^26s$, $3d^24d$ and $3d^25d$ cover the energy interval from 62 180 to 84 652 cm^{-1}. In total 253 energy levels and 1872 spectral lines ranging from 122 to 2198 nm are reported in the National Institute of Standards and technology (NIST) compilations (Saloman 2012; Kramida et al. 2014).

Experimental lifetimes in Ti II obtained with different techniques have been reported in several papers. The first investigation, by Roberts, Andersen & Sørensen (1973), used the beam-foil method to obtain lifetimes in both the 4p and 4d configurations. In Gosselin, Pinnington & Ansbacher (1987), a Ti^+ beam from a heavy ion accelerator was crossed by a laser to selectively excite the 4p $z^4D_{5/2}$ state. The reported lifetime has an uncertainty of only 1.5 per cent and remains the most accurately known lifetime in Ti II. Langhans, Schade & Helbig (1995), Kwiatkowski, Werner & Zimmermann (1985) and Bizzarri et al. (1993) employed time-resolved laser-induced fluorescence (TR-LIF) on ions from a hollow cathode discharge. The metastable states of the $3d^3$, $3d^2(^3P)4s$ and $(3d + 4s)^3$

★ E-mail: henrik.hartman@astro.lu.se (HH); lars.engstrom@fysik.lth.se (LE); Hampus.Nilsson@astro.lu.se (HN)

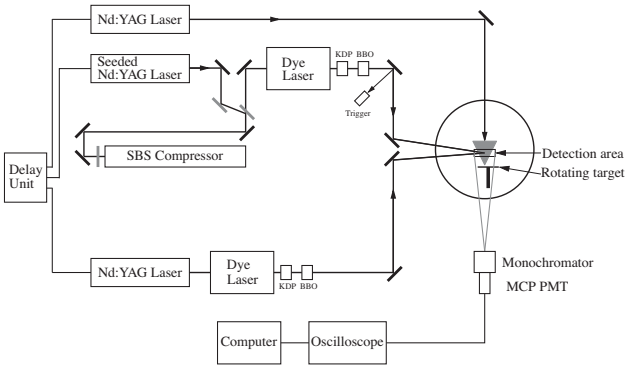

Figure 1. Experimental set-up for TR-LIF at the Lund High Power Laser Facility using two-step excitation. See discussion in text for details.

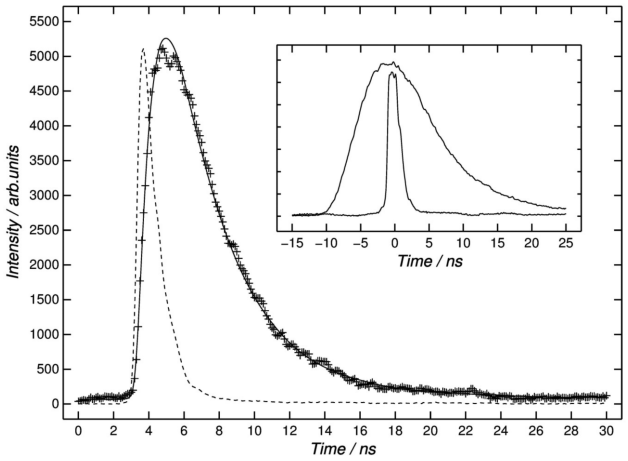

Figure 2. The first 30 ns of the decay of the 5s $e^2F_{5/2}$ level in Ti II following two-step excitation. The measured decay (+) is plotted together with a fitted single exponential function (solid line) convoluted by the recorded second step laser pulse (dashed curve). The insert shows the timing between the fluorescence from the intermediate 4p $z^2D_{3/2}$ level (broad structure) and the second step laser (narrow peak).

electron configurations of Ti II have been investigated by a laser probing technique on Ti ions in a storage ring in series of papers (Hartman et al. 2003, 2005; Palmeri et al. 2008a). Along with the lifetimes, transition probabilities for several decay channels from these metastable levels are also reported.

A number of experimental investigations of both absolute and relative transition probabilities and oscillator strengths from 4p levels have been stimulated by astrophysical observations. Various methods and spectral sources have been employed. These include absorption measurements (Wiese, Fedchak & Lawler 2001), emission studies from a shock tube (Boni 1968; Wolnik & Berthel 1973), from arc- (Tatum 1961; Roberts, Voigt & Czernichowski 1975) and spark-sources (Wobig 1962), hook method (Danzmann & Kock 1980) and Fourier transform spectroscopy (Pickering, Thorne & Perez 2001; Wood et al. 2013).

Several papers report theoretical investigations of radiative parameters in Ti II. The most recent of these are Kurucz (2011) and Ruczkowski, Elantkowska & Dembczynski (2014). Transition probabilities and oscillator strengths of Ti II spectral lines are also included in several compilations, e.g. Thévenin (1989), Savanov, Huovelin & Tuominen (1990) and Meylan et al. (1993).

This short literature survey shows that a large number of studies have been devoted to transition probabilities and radiative lifetimes for low-lying excited states, mainly belonging to the $3d^24p$ electron configuration. There are no experimental data for the high lying 5s levels that are the main subject of this work.

2 EXPERIMENT

The experimental set-up for single-step experiments at the Lund High Power Laser Facility has recently been described in detail (Engström et al. 2014), and here we focus mainly on the new features involved in the two-step process. The experimental set-up is presented in Fig. 1. The Ti ions are produced in an ablation process, where the second harmonic of an Nd:YAG laser (Continuum Surelite) with 10 ns pulses are focused on a rotating Ti target. The target is placed in a vacuum chamber with a pressure of around 10^{-4} mbar. The generated plasma is crossed by the two excitation laser beams about 1 cm above the target. With the first laser, the intermediate odd states in $3d^2(^3F)4p$, around 32 000 cm^{-1}, are excited and used as platforms for the excitation of the high-lying even parity 5s states.

The first laser channel consist of an Nd:YAG laser (Continuum NY-82) pumping a Continuum Nd-60 dye laser operating with DCM dye ($C_{19}H_{17}N_3O$). The 10 ns long pulses are frequency doubled using a KDP crystal (KH_2PO_4). For the second step, the same type of lasers and dye are used but here the Nd:YAG laser is injection seeded and the pulses are temporally compressed using stimulated Brillouin scattering in water. After frequency doubling in a KDP crystal, we obtain pulses with a typical temporal full width at half-maximum of 1.2 ns.

All three laser systems operate at 10 Hz and are synchronized by a delay generator. The delay generator allows us to set the time between the plasma generating laser and the excitation pulses (typically around 1 μs) and also the delay between the first and second excitation steps. The latter timing was checked before every measurement to ensure that the second step occurred at the maximum population of the intermediate level, as determined by the decay of this level in some channel. Since the pulses in the first step are much longer than in the second step, this also ensures that the intermediate population is almost constant during the final excitation. The timing between the two steps is illustrated in the insert in Fig. 2.

The fluorescence from the excited states was observed with a 1/8 m grating monochromator, with its 0.28 mm wide entrance slit oriented parallel to the excitation lasers, giving a line width of 0.5 nm in the second spectral order. The dispersed light was registered by a fast microchannel-plate photomultiplier tube (Hamamatsu R3809U) and digitized by a Tektronix DPO 7254 oscilloscope triggered by the second step laser pulses detected with a fast photodiode. The final decay curves and pulse shape were obtained by averaging over 1000 laser pulses. The code DECFIT (Palmeri et al. 2008b) was then used to extract the lifetimes by fitting a single exponential function convoluted by the measured shape of the second step laser pulse and a background function to the observed decay. A typical example is shown in Fig. 2.

Table 1 gives the wavelengths and excitation schemes used in the single-step measurements of four 4p levels, performed to allow a comparison with earlier experimental results. Two of these levels are also used as platforms in the two-step experiments. A complete description of the latter is given in Table 2. In the complex level system of the iron-group elements, with a parent term structure and multiple ionization limits, the strong transitions group in wavelengths due to the similar energy difference between 4s and 4p for the different parent terms (similar promotion energy). In addition, the energy difference between 4p and 5s is similar to that of 4s and

Table 1. Single-step excitation schemes for $3d^2(^3F)4p$ levels in Ti II.

Level	E^a (cm^{-1})	Starting level E^a (cm^{-1})	Excitation^b λ_{air} (nm)	λ^c_{obs} (nm)
$z^4F_{5/2}$	30 958	0	322.92	333
$z^2D_{3/2}$	31 756	0	314.80	368
$z^4D_{5/2}$	32 698	1087	316.26	307, 308, 316
$z^4D_{7/2}$	32 767	393	308.80	217

Notes. [a]Huldt et al. (1982).
[b]All levels were excited using the second harmonic of the dye laser.
[c]All fluorescence measurements were performed in the second spectral order.

Table 2. Two-step excitation schemes for $3d^2(^3F)5s$ levels in Ti II.

Final level	E^a (cm^{-1})	Intermediate level E^a (cm^{-1})	Excitation^b λ_{air} (nm)	λ^c_{obs} (nm)
$e^4F_{3/2}$	62 180	30 958	320.20	306, 319
$e^4F_{5/2}$	62 272	30 958	319.26	305, 318[d]
$e^4F_{7/2}$	62 411	31 301	321.35	319[e]
$e^4F_{9/2}$	62 595	31 301	319.46	306
$e^2F_{5/2}$	63 169	31 756	318.25	312, 349
$e^2F_{7/2}$	63 446	32 025, 32 767	318.17, 325.86	313[f], 348

Notes. [a]Huldt et al. (1982).
[b]All levels were excited using the second harmonic of the dye laser.
[c]All fluorescence measurements were performed in the second spectral order.
[d]Corrected for scattered light from the second step laser at 319 nm.
[e]Corrected for fluorescence background from first step laser at 323 nm.
[f]Corrected for fluorescence background from first step laser at 316 nm.

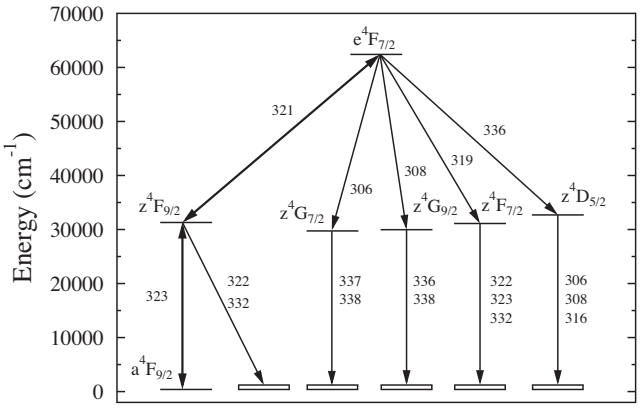

Figure 3. Decay chains from the 5s $e^4F_{7/2}$ level in Ti II. All wavelengths are given in nm. In the experiment, the 5s level is excited in two steps using the transitions at 323.4 nm (4s−4p) and 321.3 nm (4p−5s).

4p, making the transitions between these configurations also falls in the same region. For Ti II, this region is between 300 and 350 nm. Thus, the observed decay from the 5s levels under investigation might be blended with fluorescence from 4p levels. Fig. 3 presents a schematic picture using 5s $e^4F_{7/2}$ as an example. Two types of blending may be distinguished: from a direct fluorescence (4s−4p) channel from the intermediate level or from the secondary decay of a 4p level populated by the decay from the 5s level studied.

While the fluorescence from the intermediate level is very intense and observable even at a rather large wavelength off-set, its perturbing influence is easily handled by recording an additional decay curve, with the second step laser turned off to reveal the

Table 3. Lifetimes of the $3d^2(^3F)4p$ and 5s levels in Ti II.

Level	E^a (cm^{-1})	τ_{exp} (ns) Our work	τ_{exp} (ns) Other	τ_{calc} (ns) Our work	τ_{calc} (ns) Kurucz^b
4p $z^4F_{5/2}$	30 958	3.87 ± 0.20	4.1 ± 0.2[c] 4.1 ± 0.3[d]	3.76	4.15
4p $z^2D_{3/2}$	31 756	6.10 ± 0.20	6.6 ± 0.3[c] 6.3 ± 1[d] 7.8 ± 1[e]	5.87	6.85
4p $z^4D_{5/2}$	32 698	3.86 ± 0.20	4.0 ± 0.2[c] 3.9 ± 0.4[d] 5.2 ± 0.8[e] 4.01 ± 0.06[f]	3.47	3.92
4p $z^4D_{7/2}$	32 767	3.75 ± 0.20	4.0 ± 0.2[c] 4.1 ± 0.5[d]	3.40	3.85
5s $e^4F_{3/2}$	62 180	2.96 ± 0.20		3.19	2.82
5s $e^4F_{5/2}$	62 272	3.05 ± 0.20		3.19	2.82
5s $e^4F_{7/2}$	62 411	3.02 ± 0.20		3.19	2.82
5s $e^4F_{9/2}$	62 595	3.14 ± 0.20		3.19	2.82
5s $e^2F_{5/2}$	63 169	3.04 ± 0.15		3.41	3.04
5s $e^2F_{7/2}$	63 446	3.02 ± 0.15	3.0 ± 0.6[g]	3.41	3.05

Notes. [a]Huldt et al. (1982).
[b]Kurucz (2011).
[c]Bizzarri et al. (1993), TR-LIF.
[d]Kwiatkowski et al. (1985), TR-LIF.
[e]Roberts et al. (1973), beam-foil.
[f]Gosselin et al. (1987), Beam-Laser.
[g]The original assignment of this level in Roberts et al. (1973) to $3d4s(^3F)4p$ is changed to $3d^2(^3F)5s$.

blending contribution, which can be subtracted from the primary decay measurement before the lifetime analysis. Two examples of this problem were encountered and are marked in Table 2. Secondary decays, on the other hand, arise from decays along a chain from the level of interest and cannot be corrected for, but must be understood in order to choose an appropriate channel for the primary decay measurement. For example, the lifetime of 5s $e^4F_{7/2}$ is measured in the channel 319 nm, with the final result of (3.02 ± 0.20) ns, after correction for the first step fluorescence at 323 nm. However, the decay could be observed in three other sufficiently intense channels as well: 306, 308 and 336 nm. These are, however, blended by one or more secondary decays, as shown in Fig. 3. The measured lifetimes in these channels are 6.5, 3.8 and 3.3 ns, respectively, clearly demonstrating the importance of choosing an appropriate decay channel.

The final lifetimes obtained are presented in Table 3. The values represent the average of between 10 and 20 measurements performed over a number of days, and the quoted uncertainties take into account both the statistical uncertainty in the fitting process and, primarily, the variation of the results between the different measurements.

In Table 4, we have derived absolute transition probabilities and log *gf* values for 57 transitions depopulation five of the six 5s levels investigated in this work. The results are obtained by combining our experimental lifetimes in Table 3 with experimental branching fractions reported by Pickering et al. (2001).

3 THEORY

The relativistic Hartree–Fock (HFR) approach (Cowan 1981) including core-polarization (CPOL) effects by means of a model potential and a correction to the transition dipole operator (HFR + CPOL) [see e.g. Quinet et al. 1999 and Quinet et al. 2002 has been

Table 4. Transition probabilities and oscillator strengths for lines from the 5s levels measured in this work.

Upper level	Lower level	λ^a (nm)	BF^a	A^b (10^6 s^{-1})	log $gf^b_{\rm exp}$	log $gf^b_{\rm calc}$
$3d^2(^3F)5s\ e^4F_{5/2}$	$3d^2(^3F)4p\ z^2G_{5/2}$	360.530 46	0.35 ± 0.03	1.15 ± 0.12	−1.872 ± 0.045	− 1.80
62 272.16 cm^{-1}	$3d^2(^3F)4p\ z^4D_{7/2}$	338.826 30	0.15 ± 0.02	0.49 ± 0.07	−2.294 ± 0.060	− 2.19
$\tau = 3.05 \pm 0.20$ ns	$3d^2(^3F)4p\ z^4D_{5/2}$	338.034 49	5.12 ± 0.16	16.8 ± 1.2	−0.763 ± 0.030	− 0.84
	$3d^2(^3F)4p\ z^4D_{3/2}$	336.946 69	15.32 ± 0.49	50.2 ± 3.7	−0.290 ± 0.031	− 0.34
	$3d^2(^3F)4p\ z^2D_{5/2}$	330.518 39	1.25 ± 0.05	4.1 ± 0.3	−1.395 ± 0.032	− 1.54
	$3d^2(^3F)4p\ z^2D_{3/2}$	327.605 34	0.53 ± 0.03	1.74 ± 0.15	−1.775 ± 0.036	− 1.59
	$3d^2(^3F)4p\ z^2F_{7/2}$	324.777 03	0.28 ± 0.03	0.92 ± 0.12	−2.060 ± 0.051	− 2.68
	$3d^2(^3F)4p\ z^4F_{7/2}$	320.844 82	7.59 ± 0.24	24.9 ± 1.8	−0.638 ± 0.031	− 0.71
	$3d^2(^3F)4p\ z^4F_{5/2}$	319.255 68	21.68 ± 0.69	71.1 ± 5.2	−0.186 ± 0.031	− 0.18
	$3d^2(^3F)4p\ z^4F_{3/2}$	318.015 00	5.29 ± 0.17	17.3 ± 1.3	−0.802 ± 0.031	− 0.83
	$3d^2(^3F)4p\ z^4G_{5/2}$	307.245 88	37.27 ± 1.45	122.2 ± 9.3	0.016 ± 0.032	0.01
	$3d^2(^3F)4p\ z^4G_{5/2}$	305.460 55	5.15 ± 0.17	16.9 ± 1.2	−0.849 ± 0.031	− 0.85
$3d^2(^3F)5s\ e^4F_{7/2}$	$3d^2(^3P)4p\ y^4D_{5/2}$	457.971 06	0.78 ± 0.16	2.6 ± 0.6	−1.187 ± 0.085	− 1.98
62 410.78 cm^{-1}	$3d^2(^3F)4p\ z^2G_{9/2}$	361.397 66	0.28 ± 0.02	0.93 ± 0.09	−1.838 ± 0.040	− 1.76
$\tau = 3.02 \pm 0.20$ ns	$3d^2(^3F)4p\ z^4D_{7/2}$	337.242 19	3.85 ± 0.13	12.7 ± 0.9	−0.760 ± 0.031	− 0.88
	$3d^2(^3F)4p\ z^4D_{5/2}$	336.457 92	16.28 ± 0.54	53.9 ± 4.0	−0.136 ± 0.031	− 0.18
	$3d^2(^3F)4p\ z^2D_{5/2}$	329.010 96	1.42 ± 0.05	4.70 ± 0.35	−1.214 ± 0.031	− 1.10
	$3d^2(^3F)4p\ z^4F_{9/2}$	321.348 27	4.50 ± 0.15	14.9 ± 1.1	−0.734 ± 0.031	− 0.82
	$3d^2(^3F)4p\ z^4F_{7/2}$	319.424 17	27.02 ± 1.05	89.5 ± 6.9	0.039 ± 0.032	− 0.01
	$3d^2(^3F)4p\ z^4F_{5/2}$	317.849 02	5.12 ± 0.17	17.0 ± 1.3	−0.687 ± 0.031	− 0.72
	$3d^2(^3F)4p\ z^4G_{9/2}$	308.146 89	35.28 ± 1.38	117 ± 9	0.124 ± 0.032	0.14
	$3d^2(^3F)4p\ z^4G_{5/2}$	305.942 86	5.12 ± 0.17	17.0 ± 1.3	−0.721 ± 0.031	− 0.73
	$3d^2(^3F)4p\ z^4G_{5/2}$	304.172 52	0.17 ± 0.02	0.56 ± 0.08	−2.204 ± 0.055	− 2.26
$3d^2(^3F)5s\ e^4F_{9/2}$	$3d^2(^3P)4p\ y^4D_{7/2}$	458.655 99	0.10 ± 0.02	0.32 ± 0.07	−1.998 ± 0.083	− 1.85
62 595.03 cm^{-1}	$3d^2(^3F)4p\ z^4D_{7/2}$	335.159 47	20.00 ± 0.80	63.7 ± 4.8	0.030 ± 0.031	0.04
$\tau = 3.14 \pm 0.20$ ns	$3d^2(^3F)4p\ z^2F_{7/2}$	321.406 67	0.48 ± 0.02	1.53 ± 0.12	−1.626 ± 0.032	− 1.71
	$3d^2(^3F)4p\ z^4F_{9/2}$	319.456 71	30.05 ± 1.20	95.7 ± 7.2	0.166 ± 0.031	0.18
	$3d^2(^3F)4p\ z^4F_{7/2}$	317.555 11	3.18 ± 0.11	10.1 ± 0.7	−0.815 ± 0.030	− 0.85
	$3d^2(^3F)4p\ z^4G_{11/2}$	308.988 92	42.53 ± 1.70	135 ± 10	0.287 ± 0.031	0.26
	$3d^2(^3F)4p\ z^4G_{9/2}$	306.407 11	3.50 ± 0.12	11.1 ± 0.8	−0.804 ± 0.030	− 0.85
	$3d^2(^3F)4p\ z^4G_{5/2}$	304.227 86	0.16 ± 0.02	0.51 ± 0.07	−2.151 ± 0.057	− 2.37
$3d^2(^3F)5s\ e^2F_{5/2}$	$3d^2(^3P)4p\ x^2D_{3/2}$	547.666 64	0.65 ± 0.21	2.1 ± 0.7	−1.239 ± 0.123	− 1.40
63 169.02 cm^{-1}	$3d^2(^1G)4p\ y^2G_{5/2}$	514.568 99	1.02 ± 0.08	3.4 ± 0.3	−1.097 ± 0.038	− 1.04
$\tau = 3.04 \pm 0.15$ ns	$3d^2(^1D)4p\ y^2F_{5/2}$	430.129 59	1.82 ± 0.11	6.0 ± 0.5	−1.002 ± 0.033	− 1.29
	$3d^2(^1D)4p\ y^2D_{3/2}$	424.216 59	0.31 ± 0.06	1.02 ± 0.20	−1.782 ± 0.079	− 1.53
	$3d^2(^1D)4p\ y^2D_{5/2}$	421.961 68	0.43 ± 0.05	1.41 ± 0.18	−1.645 ± 0.052	− 1.13
	$3d^2(^1D)4p\ z^2P_{3/2}$	417.668 55	1.03 ± 0.09	3.39 ± 0.34	−1.274 ± 0.042	− 2.13
	$3d^2(^3F)4p\ z^2G_{5/2}$	349.236 37	41.04 ± 1.30	135.0 ± 7.9	0.171 ± 0.025	0.10
	$3d^2(^3F)4p\ z^4D_{5/2}$	328.086 38	0.40 ± 0.06	1.32 ± 0.21	−1.895 ± 0.064	− 2.00
	$3d^2(^3F)4p\ z^4D_{3/2}$	327.061 65	1.30 ± 0.07	4.28 ± 0.31	−1.386 ± 0.031	− 1.39
	$3d^2(^3F)4p\ z^2D_{3/2}$	318.253 07	17.15 ± 0.54	56.4 ± 3.3	−0.289 ± 0.025	− 0.35
	$3d^2(^3F)4p\ z^2F_{7/2}$	315.583 32	1.47 ± 0.07	4.84 ± 0.33	−1.363 ± 0.029	− 1.37
	$3d^2(^3F)4p\ z^2F_{5/2}$	312.784 98	32.11 ± 1.01	105.6 ± 6.2	−0.032 ± 0.025	− 0.05
	$3d^2(^3F)4p\ z^4F_{5/2}$	310.367 47	0.18 ± 0.06	0.59 ± 0.20	−2.290 ± 0.126	− 3.80
	$3d^2(^3F)4p\ z^4F_{3/2}$	309.194 94	0.26 ± 0.05	0.86 ± 0.17	−2.133 ± 0.079	− 2.79
	$3d^2(^3F)4p\ z^4G_{5/2}$	297.314 17	0.20 ± 0.07	0.66 ± 0.23	−2.281 ± 0.131	− 2.52
$3d^2(^3F)5s\ e^2F_{7/2}$	$3d^2(^3P)4p\ x^2D_{5/2}$	539.120 20	0.56 ± 0.08	1.85 ± 0.28	−1.190 ± 0.061	− 1.20
63 445.88 cm^{-1}	$3d^2(^1G)4p\ y^2G_{9/2}$	508.374 07	1.26 ± 0.09	4.17 ± 0.36	−0.888 ± 0.036	− 0.91
$\tau = 3.02 \pm 0.15$ ns	$3d^2(^1D)4p\ y^2F_{5/2}$	425.064 49	0.25 ± 0.03	0.83 ± 0.11	−1.746 ± 0.053	− 1.39
	$3d^2(^1D)4p\ y^2D_{5/2}$	417.086 31	0.83 ± 0.06	2.75 ± 0.24	−1.242 ± 0.037	− 1.82
	$3d^2(^3F)4p\ z^2G_{9/2}$	348.362 46	39.53 ± 1.27	130.9 ± 7.7	0.280 ± 0.025	0.21
	$3d^2(^3F)4p\ z^2G_{5/2}$	345.889 96	1.12 ± 0.05	3.71 ± 0.25	−1.274 ± 0.028	− 1.35
	$3d^2(^3F)4p\ z^4D_{7/2}$	325.863 64	0.62 ± 0.05	2.05 ± 0.19	−1.583 ± 0.039	− 1.78
	$3d^2(^3F)4p\ z^4D_{5/2}$	325.131 43	2.55 ± 0.10	8.44 ± 0.53	−0.970 ± 0.027	− 1.02
	$3d^2(^3F)4p\ z^2D_{5/2}$	318.172 19	18.96 ± 0.61	62.8 ± 3.7	−0.118 ± 0.025	− 0.19
	$3d^2(^3F)4p\ z^2F_{7/2}$	312.848 33	31.27 ± 1.00	103.5 ± 6.1	0.085 ± 0.025	0.07
	$3d^2(^3F)4p\ z^4G_{9/2}$	298.619 16	0.44 ± 0.05	1.46 ± 0.18	−1.807 ± 0.051	− 1.72

Notes. [a]Pickering et al. (2001).
[b]This work.

used to compute the transition probabilities in Ti II. The following 27 configurations have been considered explicitly in our physical model: $3d^3$, $3d^24s$, $3d^25s$, $3d^26s$, $3d^24d$, $3d^25d$, $3d4s^2$, $3d4p^2$, $3d4d^2$, 3d4s4d, 3d4s5d, 3d4s5s, $4s^24d$, $4s^25d$, $4s^25s$ (even parity) and $3d^24p$, $3d^25p$, $3d^24f$, $3d^25f$, 3d4s4p, 3d4s5p, 3d4s4f, 3d4s5f, $4s^24p$, $4s^25p$, $4s^24f$, $4s^25f$ (odd parity). The ionic core considered for the CPOL was an argon-like core, i.e. a $3p^6$ Ti V core. The dipole polarizability, α_d, for such a core is 1.48 a_0^3, according to Johnson,

Table 5. Radial parameters adopted in the HFR+CPOL calculations for the $3d^3$, $3d^24s$, $3d^25s$, $3d^24d$ and $3d4s^2$ even-parity configurations of Ti II.

Configuration	Parameter	Ab initio E (cm^{-1})	Fitted E (cm^{-1})	Ratio	Note[a]
$3d^3$	E_{av}	15 742	12 262		
	$F^2(3d,3d)$	56 469	44 972	0.796	
	$F^4(3d,3d)$	34 782	24 920	0.716	
	α	0	−22		
	β	0	486		
	ζ_{3d}	102	102	1.000	F
$3d^24s$	E_{av}	8511	8295		
	$F^2(3d,3d)$	65 280	50 087	0.767	
	$F^4(3d,3d)$	40 580	31 161	0.768	
	α	0	37		
	β	0	153		
	ζ_{3d}	125	125	1.000	F
	$G^2(3d,4s)$	10 847	8084	0.745	R1
$3d^25s$	E_{av}	69 222	69 392		
	$F^2(3d,3d)$	67 340	51 820	0.770	
	$F^4(3d,3d)$	41 960	30 640	0.730	
	α	0	35		F
	β	0	150		F
	ζ_{3d}	129	129	1.000	F
	$G^2(3d,5s)$	2009	1497	0.745	R1
$3d^24d$	E_{av}	73 261	74 068		
	$F^2(3d,3d)$	67 349	53 704	0.797	
	$F^4(3d,3d)$	41 970	32 667	0.778	
	α	0	35		F
	β	0	150		F
	ζ_{3d}	129	129	1.000	F
	ζ_{4d}	9	9	1.000	F
	$F^2(3d,4d)$	6812	3961	0.581	
	$F^4(3d,4d)$	3087	1999	0.647	
	$G^0(3d,4d)$	5311	2374	0.447	R2
	$G^2(3d,4d)$	3562	1593	0.447	R2
	$G^4(3d,4d)$	2417	1081	0.447	R2
$3d4s^2$	E_{av}	30 013	30 791		
	ζ_{3d}	149	140	0.945	
$3d^3$–$3d^24s$	$R^2(3d,3d;3d,4s)$	−9870	−7356	0.745	

Note. [a]F: fixed parameter value; Rn : fixed ratio between these parameters.

Kolb & Huang (1983). For the cut-off radius, we used the HFR mean value of the outermost 3p core orbital, i.e. 1.08 a_0.

Radial integrals of the $3d^3$, $3d^24s$, $3d^25s$, $3d^24d$, $3d4s^2$, $3d^24p$ and 3d4s4p, considered as free parameters, were then adjusted with a well-established least-squares optimization program minimizing the discrepancies between the calculated Hamiltonian eigenvalues and the experimental energy levels taken from Huldt et al. (1982). More precisely, the average energies (E_{av}), the electrostatic direct (F^k) and exchange (G^k) integrals, the spin-orbit (ζ_{nl}) and effective interaction parameters (α and β) were allowed to vary during the fitting process. We also adjusted the Configuration Interaction (CI) parameters (R^k) between the $3d^3$ and $3d^24s$ even configurations and between the $3d^24p$ and 3d4s4p odd configurations. For parameters belonging to other configurations, a scaling factor of 0.80 was applied.

The numerical values of the parameters adopted in the present calculations are reported in Tables 5 and 6 for even and odd-parity configurations, respectively. This semi-empirical process led to average deviations with experimental energy levels equal to 125 cm^{-1} (even parity) and 78 cm^{-1} (odd parity).

Table 6. Radial parameters adopted in the HFR+CPOL calculations for the $3d^24p$ and 3d4s4p odd-parity configurations of Ti II.

Configuration	Parameter	Ab initio E (cm^{-1})	Fitted E (cm^{-1})	Ratio	Note[a]
$3d^24p$	E_{av}	37 888	38 418		
	$F^2(3d,3d)$	66 208	50 859	0.768	
	$F^4(3d,3d)$	41 202	29 899	0.726	
	α	0	49		
	β	0	85		
	ζ_{3d}	127	127	1.000	F
	ζ_{4p}	176	176	1.000	F
	$F^2(3d,4p)$	14 522	11 668	0.803	
	$G^1(3d,4p)$	6343	5603	0.883	
	$G^3(3d,4p)$	5111	3249	0.636	
3d4s4p	E_{av}	56 603	59 030		
	ζ_{3d}	150	150	1.000	F
	ζ_{4p}	236	236	1.000	F
	$F^2(3d,4p)$	15 975	14 378	0.900	
	$G^2(3d,4s)$	10 055	8363	0.832	
	$G^1(3d,4p)$	9785	6346	0.649	
	$G^3(3d,4p)$	5244	3136	0.598	
	$G^1(4s,4p)$	38 957	25 804	0.662	
$3d^24p$–3d4s4p	$R^2(3d,3d;3d,4s)$	−6658	−4420	0.664	R
	$R^2(3d,4p;4s,4p)$	−13 417	−8906	0.664	R
	$R^1(3d,4p;4s,4p)$	−13 786	−9152	0.664	R

Note. [a]F: fixed parameter value; R: fixed ratio between these parameters.

4 RESULTS AND DISCUSSION

Table 3 shows that our lifetimes for the 4p levels agree with the previous investigations using laser excitation within the mutual error bars. Although there is a tendency for the new results to be somewhat shorter. Compared with the old values obtained by the beam-foil technique by Roberts et al. (1973), we note a significant discrepancy. This is most likely caused by the combined problem of line blending and cascades from higher lying states caused by the non-selective excitation in the beam-foil process. In the case of the $3d^25s\ e^2F_{7/2}$ level, Roberts et al. (1973) measured the lifetime using a transition at 348.4 nm, but assigned the value to the configuration 3d4s4p. This is most likely a typographical error since e^2F denotes an even configuration. The line at 348.4 nm is an intense transition used in this work to measure the $5s\ e^2F_{7/2}$ level (Table 2) and we believe that the assignment by Roberts et al. (1973) should be changed. Doing so also results in agreement between the measured lifetimes.

The computed radiative lifetimes obtained in this work are compared with our experimental values in Table 3. As shown in this table, the overall agreement between theory and experiment is very good (within 10 per cent). For comparison, Table 3 includes the theoretical lifetimes obtained by Kurucz (2011). This work also used a semi-empirical approach based on a superposition of configurations calculation with a modified version of the Cowan (1981) codes and experimental level energies. We note a very good qualitative agreement between the two calculations.

Table 7 gives the HFR+CPOL oscillator strengths (log *gf*) and weighted transition probabilities (*gA*), obtained in this work, for 3336 Ti II spectral lines from 138 to 9966 nm, combining lower levels in the range 0–74 000 cm^{-1} and upper levels 30 000–80 000 cm^{-1}. Only transitions with log $gf > -4$ are reported in the table in which we also give, in the last column, the value of the cancellation factor (CF), as defined by Cowan (1981). Very small values of this factor (typically < 0.05) indicate strong cancellation effects in the calculation of the line strengths and the corresponding

Table 7. Radiative transition rates for Ti II spectral lines. The full table is available online.

	Lower level[b]			Upper level[b]			Previous works				This work		
λ (nm)[a]	E (cm^{-1})	Parity	J	E (cm^{-1})	Parity	J	log gf[c]	log gf[d]	log gf[e]	log gf[f]	log gf	gA (s^{-1})	CF
138.1535	226	(e)	3.5	72 609	(o)	3.5		−2.72			−3.21	2.16E+06	0.092
138.2025	94	(e)	2.5	72 452	(o)	2.5		−2.61			−3.11	2.71E+06	0.096
138.2395	0	(e)	1.5	72 338	(o)	1.5		−2.73			−3.23	2.03E+06	0.101
138.3689	0	(e)	1.5	72 271	(o)	0.5		−2.32			−2.83	5.10E+06	0.119
138.4196	94	(e)	2.5	72 338	(o)	1.5		−2.11			−2.62	8.26E+06	0.114
138.4543	226	(e)	3.5	72 452	(o)	2.5		−1.93			−2.44	1.25E+07	0.112
138.4744	393	(e)	4.5	72 609	(o)	3.5		−1.77			−2.29	1.77E+07	0.111
139.0478	1216	(e)	4.5	73 134	(o)	4.5		−3.76			−3.71	6.69E+05	0.111
139.6159	984	(e)	2.5	72 609	(o)	3.5		−3.77			−3.43	1.28E+06	0.294
139.7573	393	(e)	4.5	71 946	(o)	5.5		−2.88			−2.37	1.47E+07	0.077
–	–	–	–	–	–	–	–	–	–	–	–	–	

Notes. [a]Wavelengths (in vacuum/air below/above 200 nm) deduced from experimental energy levels.
[b]Experimental energy levels taken from Huldt et al. (1982) and Saloman (2012). (e) and (o) stand for 'even' and 'odd', respectively.
[c]Pickering et al. (2001).
[d]Kurucz (2011).
[e]Wood et al. (2013).
[f]Ruczkowski et al. (2014).

transition rates can be affected by larger uncertainties and should be considered with some care. However, only about 15 per cent of the total number of lines reported in Table 7 are affected by strong cancellation effects (CF < 0.05) and it is clear that most of these lines are characterized by very weak oscillator strengths (typically log $gf < -2$). It is difficult to estimate the uncertainties of the computed radiative rates for such transitions which are extremely sensitive to small changes in the atomic wavefunctions but, according to Cowan (1981), it is expected that very strong cancellation effects can lead to errors in the line strength calculations ranging from 50 percent to one or more orders of magnitude.

In the same table, we list the most recent oscillator strengths published by Pickering et al. (2001), Kurucz (2011), Wood et al. (2013), and Ruczkowski et al. (2014). In the work of Pickering et al. (2001), the relative intensities of Ti II emission lines between 187 and 602 nm from 89 levels were measured by high-resolution Fourier transform spectrometry, using a hollow cathode lamp as light source. The branching fractions were then combined with 39 measured and 44 computed lifetimes to give absolute transition probabilities for 624 lines. Fig. 4 shows the good agreement between our calculated log gf values and the values from Pickering et al. (2001), particularly when they used experimental lifetimes (filled circles).

Table 4 gives a more detailed comparison between our calculated log gf values and those obtained by combining the new experimental lifetimes in Table 3 with the branching fractions measured by Pickering et al. (2001). A very good agreement is observed, in particular for the strongest transitions for which both sets of results agree within 10–20 per cent. The average deviation in the log gf values is 0.1 with a standard deviation of 0.3.

In the analysis of Wood et al. (2013), atomic transition probability measurements for 364 lines in the UV to near-IR are reported. They were obtained from branching fraction measurements using a Fourier transform spectrometer and an echelle spectrometer combined with published radiative lifetimes. A comparison between these values and our calculated log gf values is shown in Fig. 5, and we note again the consistency between the calculated and observed values.

Kurucz (2011) used a similar semi-empirical HFR model as the one considered in our work but without inclusion of CPOL. More recently, Ruczkowski et al. (2014) used a semi-empirical oscillator strength parametrization method to compute 1340 log gf values for spectral lines in Ti II. As seen in Table 7, our new gf values are in rather good agreement with these last results, in particular for the strongest lines (log $gf > -1$), for which the typical average deviations are found to be within 20 per cent.

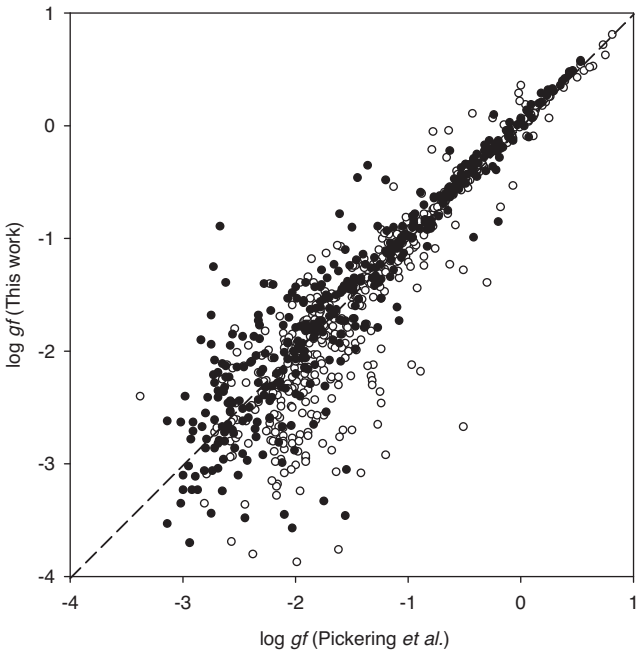

Figure 4. Comparison between the oscillator strengths (log gf) calculated in the present work and those published by Pickering et al. (2001). The circles correspond to the combination of measured branching fractions with experimental (black) and theoretical (white) lifetimes in Pickering et al. (2001).

5 CONCLUSIONS

We report new experimental radiative lifetimes of 10 4p and 5s levels in singly ionized titanium. The measurements are performed

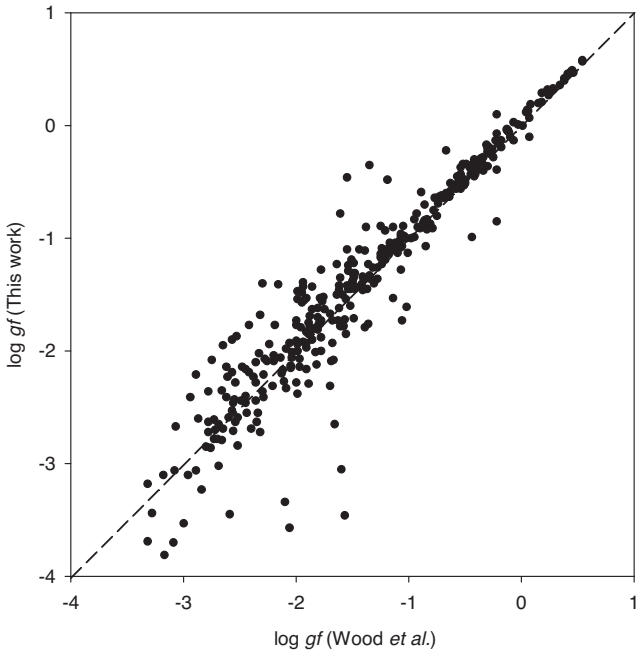

Figure 5. Comparison between the oscillator strengths (log *gf*) calculated in the present work and those published by Wood et al. (2013).

using TR-LIF on ions produced by laser ablation. One- and two-step photon excitation is employed to reach the 4p and 5s levels, respectively. For five of the six measured 5s levels, we have combined our lifetimes with the experimental branching fractions measured previously by Pickering et al. (2001) to obtain 57 experimental absolute transition probabilities and log *gf* values. In addition, we report calculated transition probabilities for 3336 Ti II spectral lines from 138 to 9966 nm. Where possible to compare, we find a good agreement with previous experiments and calculations. The transition probabilities are needed for accurate abundance determinations in astronomical objects.

ACKNOWLEDGEMENTS

This work has received funding from LASERLAB-EUROPE (grant agreement no. 284464, EC's Seventh Framework Programme), the Swedish Research Council through the Linnaeus grant to the Lund Laser Centre and a project grant 621-2011-4206, and the Knut and Alice Wallenberg Foundation. PP and PQ are, respectively, Research Associate and Research Director of the Belgian National Fund for Scientific Research F.R.S.-FNRS from which financial support is gratefully acknowledged. VF, PP, PQ, GM, and KB are grateful to the colleagues from Lund Laser Center for their kind hospitality and support. We thank the anonymous referee for careful reading of the manuscript and valuable suggestions.

REFERENCES

Bizzarri A., Huber M. C. E., Noels A., Grevesse N., Bergeson S. D., Tsekeris P., Lawler J. E., 1993, A&A, 273, 707
Boni A. A., Jr, 1968, J. Quant. Spectrosc. Radiat. Transfer, 8, 1385
Cowan R. D., 1981, The Theory of Atomic Structure and Spectra. Univ. California Press, Berkeley
Danzmann K., Kock M., 1980, J. Phys. B, 13, 2051
Engström L., Lundberg H., Nilsson H., Hartman H., Bäckström E., 2014, A&A, 570, A34
Gosselin R. N., Pinnington E. H., Ansbacher W., 1987, Phys. Lett. A, 123, 175
Hartman H. et al., 2003, J. Phys. B, 36, L197
Hartman H., Gull T., Johansson S., Smith N., HST Eta Carinae Treasury Project Team, 2004, A&A, 419, 215
Hartman H. et al., 2005, MNRAS, 361, 206
Huldt S., Johansson S., Litzén U., Wyart J.-F., 1982, Phys. Scr., 25, 401
Johnson W. R., Kolb D., Huang K. N., 1983, At. Data Nucl. Data Tables, 28, 333
Kramida A., Ralchenko Yu., Reader J. NIST ASD Team 2014, NIST Atomic Spectra Database (ver. 5.2). Available at: http://physics.nist.gov/asd
Kurucz R., 2011, Available at: http://kurucz.harvard.edu/atoms/2201/life2201.dat
Kwiatkowski M., Werner K., Zimmermann P., 1985, Phys. Rev. A, 31, 2695
Langhans G., Schade W., Helbig V., 1995, Z. Phys. D, 34, 151
Meylan T., Furenlid I., Wiggs M. S., Kurucz R. L., 1993, Astrophys. J. Suppl. Ser., 85, 163
Palmeri P. et al., 2008, J. Phys. B, 41, 125703
Palmeri P., Quinet P., Fivet V., Biémont É., Nilsson H., Engström L., Lundberg H., 2008, Phys. Scr., 78, 015304
Pickering J. C., Thorne A. P., Perez R., 2001, ApJS, 132, 403
Quinet P., Palmeri P., Biémont É., McCurdy M. M., Rieger G., Pinnington E. H., Wickliffe M. E., Lawler J. E., 1999, MNRAS, 307, 934
Quinet P., Palmeri P., Biémont É., Li Z. S., Zhang Z. G., Svanberg S., 2002, J. Alloys Compd., 344, 255
Roberts J. R., Andersen T., Sørensen G., 1973, ApJ, 181, 567
Roberts J. R., Voigt P. A., Czernichowski A., 1975, ApJ, 197, 791
Ruczkowski J., Elantkowska M., Dembczynski J., 2014, J. Quant. Spectrosc. Radiat. Transfer, 149, 168
Saloman E. B., 2012, J. Phys. Chem. Ref. Data, 41, 013101
Savanov I. S., Huovelin J., Tuominen I., 1990, A&AS, 86, 531
Sneden C., Cowan J. J., Kobayashi C., Pignatari M., Lawler J. E., Den Hartog E. A., Wood M. P., 2016, ApJ, 817, 53
Tatum J. B., 1961, MNRAS, 122, 311
Thévenin F., 1989, A&AS, 77, 137
Wiese L. M., Fedchak J. A., Lawler J. E., 2001, ApJ, 547, 1178
Wobig K. H., 1962, Z. Astrophys., 55, 100
Wolnik S. J., Berthel R. O., 1973, ApJ, 179, 665
Wood M. P., Lawler J. E., Sneden C., Cowan J. J., 2013, ApJS, 208, 27

SUPPORTING INFORMATION

Additional Supporting Information may be found in the online version of this article:

Table 7. Radiative transition rates for Ti II spectral lines. (http://www.mnras.oxfordjournals.org/lookup/suppl/doi:10.1093/mnras/stw922/-/DC1).

Please note: Oxford University Press is not responsible for the content or functionality of any supporting materials supplied by the authors. Any queries (other than missing material) should be directed to the corresponding author for the article.

This paper has been typeset from a TEX/LATEX file prepared by the author.